ACS APPLIED MATERIALS & INTERFACES

Research Article

www.acsami.org

Open Access on 08/04/2015

Structure–Property Relationship Study of Substitution Effects on Isoindigo-Based Model Compounds as Electron Donors in Organic Solar Cells

Yi Ren,[†,‡] Anna M. Hiszpanski,[†] Luisa Whittaker-Brooks,[†] and Yueh-Lin Loo*[,†,‡]

[†]Department of Chemical and Biological Engineering and [‡]Princeton Center for Complex Materials, Princeton University, Princeton, New Jersey 08544, United States

Supporting Information

ABSTRACT: We designed and synthesized a series of isoindigo-based derivatives to investigate how chemical structure modification at both the 6,6′- and 5,5′-positions of the core with electron-rich and electron-poor moieties affect photophysical and redox properties as well as their solid-state organization. Our studies reveal that 6,6′-substitution on the isoindigo core results in a stronger intramolecular charge transfer band due to strong electronic coupling between the 6,6′-substituent and the core, whereas 5,5′-substitution induces a weaker CT band that is more sensitive to the electronic nature of the substituents. In the solid state, 6,6′-derivatives generally form *J*-aggregates, whereas 5,5′-derivatives form *H*-aggregates. With only two branched ethylhexyl side chains, the 6,6′-derivatives form organized lamellar structures in the solid state. The incorporation of electron-rich benzothiophene, **BT**, substituents further enhances ordering, likely because of strong intermolecular donor–acceptor interactions between the **BT** substituent and the electron-poor isoindigo core on neighboring compounds. Collectively, the enhanced photophysical properties and solid-state organization of the 6,6′-benzothiophene substituted isoindigo derivative compared to the other isoindigo derivatives examined in this study resulted in solar cells with higher power conversion efficiencies when blended with a fullerene derivative.

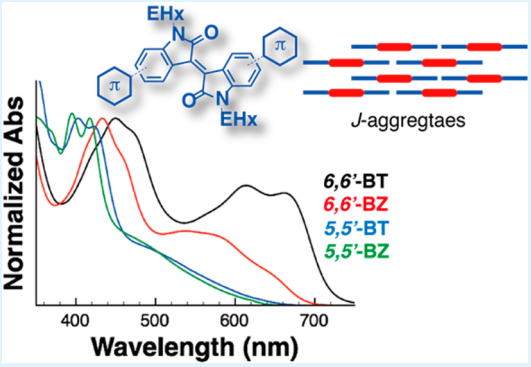

KEYWORDS: *Isoindigo, photophysics, J-aggregation, solid-state organization, organic solar cells*

INTRODUCTION

With well-defined chemical and optoelectronic properties, organic π-conjugated small molecules have been studied extensively for use in organic photovoltaics (OPVs).[1−3] A successful approach to the synthesis of such molecular systems entails the creation of donor–acceptor type structures, having both electron-donating and electron-withdrawing moieties.[4−7] Diverse chemical modification of the donor and acceptor moieties has enabled fine-tuning of the electronic structure of the compounds, including placements of the highest occupied molecular orbital, HOMO, and lowest unoccupied molecular orbital, LUMO, energy levels, their optical absorption and fluorescence as well as intermolecular charge transfer. Altering the chemistries of the donor and acceptor moieties can also dramatically affect the self-assembly of these compounds in the solid state.[8−11] Among the famous electron-withdrawing moieties, 2,1,3,-bezothiadiazole (BTD) and diketopyrrolopyrrole (DPP) conjugated cores have been extensively studied as building blocks for donor–acceptor type molecular and polymeric donors for OPVs.[5−7] Simple chemical modification of these donor–acceptor structures, such as derivatization of the conjugated cores, extension of the conjugated backbones, and addition of different terminal groups, has shown to be effective means of modifying the properties of BTD- and DPP-containing molecular semiconductors. The optical band gap, the placements of HOMO and LUMO, and structure development in the solid state have all been reported to vary drastically with such chemical modifications. Understandably, these characteristics all contribute to the performance of functional devices that incorporate these organic π-conjugated small molecules. Nguyen and co-workers, for example, uncovered that different terminal groups on DPP-based molecular semiconductors can significantly affect their phase separation characteristics when mixed with fullerene derivatives to form bulk-heterojunction active layers in solar cells, ultimately influencing device characteristics.[8,9] In another of the many examples in the literature, Bazan's group has demonstrated that the different placements of nitrogen in the BTD moiety can dramatically impact the net dipole moment of the derivatives, which results in substantial differences in the molecular organization in the solid state, and ultimately affecting OPV performance.[12]

Received: June 16, 2014
Accepted: August 4, 2014
Published: August 4, 2014

Chart 1. Isoindigo-Based Small Molecules and Polymers

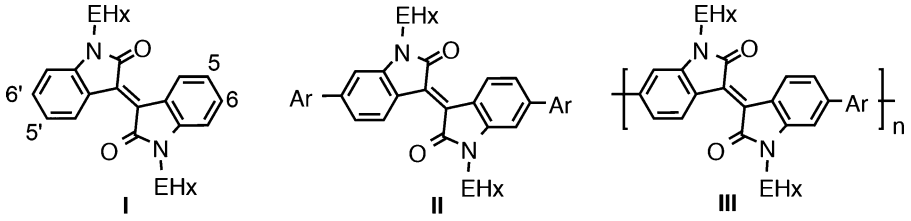

Ar: electron donating moieties

Among the electron-accepting moieties, the isoindigo core (Chart 1, I) was recently introduced as an acceptor unit for designing donor−acceptor-type molecular (see II in Chart 1) and polymeric semiconductors (see III in Chart 1) for applications in organic solar cells.[13−19] Recently, Deng and co-workers synthesized small-bandgap conjugated polymers comprising the isoindigo core as polymer donors for solar cells; bulk-heterojunction devices with a fullerene derivative yielded power conversion efficiencies, PCEs, as high as 8%.[20] In comparison, efforts to design molecular semiconductors based on isoindigo−by incorporating electron-rich substitutions, such as benzofuran, aniline, and thiophene derivatives−have unfortunately not resulted in markedly more effective donor compounds for OPVs where the PCE has remained around 2% in the absence of any additives.[21−25] Compared to more successful molecular semiconductors, such as those that incorporate DPP, the details of how chemical modification affects electronic structure and solid-state organization of isoindigo-based molecular derivatives remain unclear. Yet, to properly tailor the chemical/electronic structures of isoindigo-based derivatives for desired functionality, it is critical that we understand the structure−property relationships that are presently still lacking in the literature.

As an important electronic moiety, isoindigo offers strong intramolecular charge transfer, ICT, an essential feature for small-bandgap donor−acceptor systems.[26] Previously, electron-rich groups at the 6,6′-positions of the isoindigo core (Chart 1, I), have led to stronger low-energy charge-transfer bands compared to that exhibited by the parent compound.[13,27] It is, however, unclear how substitution at the 5,5′-positions impacts molecular properties and molecular organization. Importantly, the electronic nature of the substituent (i.e., the incorporation of an electron-poor, as opposed to an electron-rich moiety) should also affect electronic structure, particularly the ICT state, of isoindigo-based small molecules. Yet, variations in the position and the electronic nature of the substituents have not been systematically investigated or correlated with molecular organization/morphology or device performance. Although such studies have been conducted for other donor−acceptor type systems, such structure−function correlations are typically not generalizable across families of organic semiconductors with disparate chemistries. In this contribution, we investigated the structure−property relationships of a series of new model compounds containing the isoindigo core by addressing these two parameters. We find them both to play important roles in dictating device performance in OPVs. The structure−property relationships gleaned from our study brings about new insight for the design and synthesis of new isoindigo-based molecular semiconductors that yield higher PCEs when incorporated in solar cells.

EXPERIMENTAL SECTION

General. All manipulations were carried out under a dry nitrogen atmosphere employing standard Schlenk techniques. Commercially available chemicals were purchased from Sigma-Aldrich, Alfa-Aesar, and were, unless otherwise noted, used as-received. NMR solvents were purchased from Cambridge Isotope Laboratories. ^{1}H NMR and ^{13}C{1H}-NMR, were recorded on Bruker Avance (III) 300 and 500 MHz spectrometers. Chemical shifts were referenced to external TMS (^{13}C, ^{1}H). High-resolution mass spectra were run on a JEOL JMS-HX110*A*/110A tandem mass spectrometer. UV−vis−NIR experiments were carried out on a UV−vis-NIR Cary 500 spectrophotometer. AFM was performed with a Veeco Dimension NanoMan microscope operated in tapping mode. Theoretical calculations were carried out at the B3LYP/6-31G(d) level using the GAUSSIAN 03 suite of programs.[28]

6,6′- and 5,5′-substituted isoindigo derivatives were synthesized to evaluate how placement of the substituents affects molecular properties. The 6,6′-dibromo precursor, **6,6′-Br,** was prepared following reported procedures.[13] Benzothiophene-, **BT**, and benzothiazole-substituted **BZ**, isoindigo derivatives **6,6′-BT/BZ** and **5,5′-BT/Bz** were obtained via Suzuki and Stille coupling reactions. The synthesis details of these compounds can be found in the Supporting Information.

Device Fabrication. Patterned ITO (15 Ω/sq) on glass substrates was coated with 30 nm thick poly(3,4-ethylenedioxythiophene):poly(styrenesulfonate), PEDOT:PSS (Clevios P), followed by thermal annealing at 150 °C for 10 min. The PEDOT:PSS was diluted with distilled water at a 1:1 volume ratio prior to use. A 80−90 nm thick film of the donor and acceptor blend was obtained by spin-coating solutions of the new isoindigo derivatives and phenyl-C_{70}-butyric acid methyl ester ($PC_{71}BM$) at 1500 rpm for 30 s atop the PEDOT:PSS layer. The total concentration of donor and acceptor in these solutions was kept constant at 20 mg/mL in $CHCl_3$; the relative fraction of donor and acceptor was varied as detailed in Results and Discussion below. Aluminum (60 nm) top electrodes were thermally evaporated through a shadow mask at a pressure of 10^{-6} bar and an evaporation rate of 0.8 Å/s to define an active area of 0.18 cm^2. Current density−voltage (J-V) characteristics were acquired using a Keithley 2635 source measurement unit under AM 1.5G 100 mW/cm^2 illumination in a nitrogen-filled glovebox (<0.1 ppm of O_2 and H_2O). Both hole and electron mobilities of the blends were extracted from space charge limited current (SCLC) measurements on hole- and electron-only devices, respectively. The hole-only devices use PEDOT:PSS and gold as electrodes, whereas the electron-only devices use aluminum as electrodes.

GIXD experiments were conducted at the G1 station of the Cornell High Energy Synchrotron Source. The beam was selected to be 0.05 mm tall and 1 mm wide. The width of the samples was 0.5 to 0.7 cm; this smaller sample width was chosen to reduce geometric smearing of the peaks on the detector.[29] The beam energy was selected with synthetic multilayer optics (W/B4C, 23.6 Å *d*-spacing). The X-ray beam was aligned above the film's critical angle and below that of the substrate's, at 0.17° with respect to the substrate. Scattered intensity was collected with a two-dimensional CCD detector. We conducted the GIXD experiments over three separate trips to Cornell. On the first trip, the X-ray energy at the G1 station was 10.0 keV and the

Scheme 1. Synthesis of 6,6′- and 5,5′-Substituted Isoindigo Model Compounds

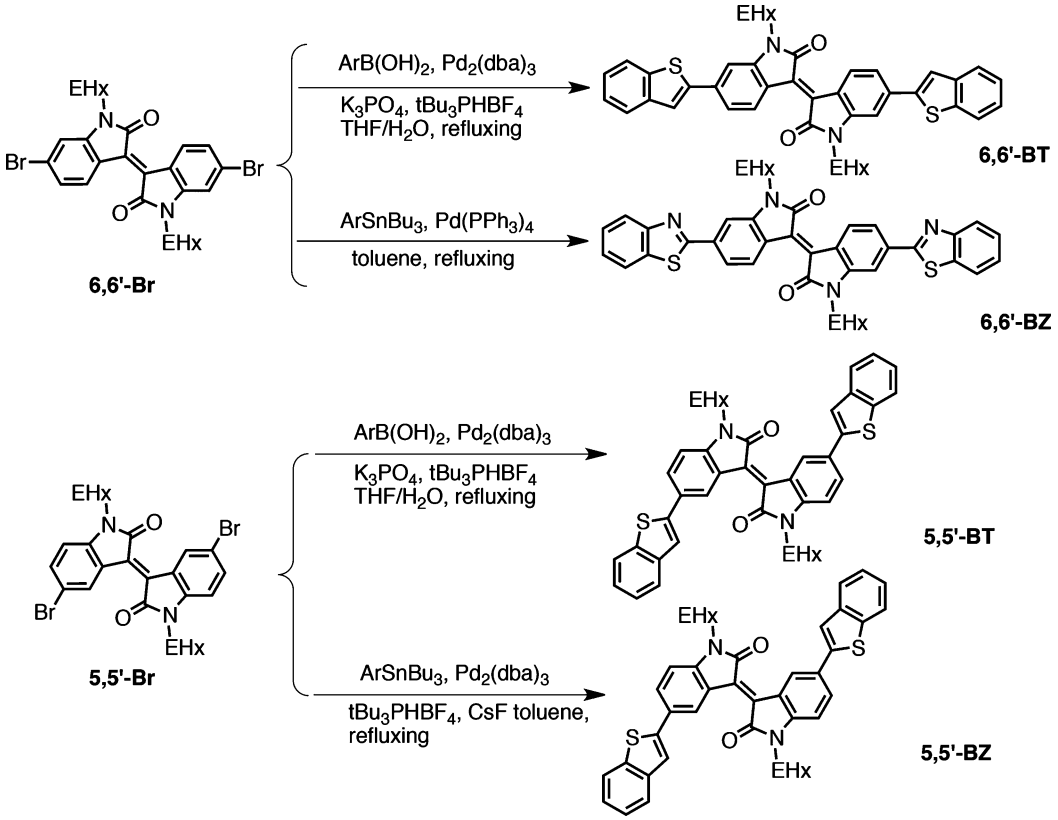

detector-to-sample distance was 97.2 mm. On the second trip, the X-ray energy was 10.6 keV with a detector-to-sample distance of 117.6 mm. On the third trip, the X-ray energy was 9.9 keV with a detector-to-sample distance of 112.0 mm. These differences were normalized and accounted for during data processing. Additionally, all GIXD images have been background subtracted, and polarization and absorption corrections were applied, though these corrections were generally small.[29]

RESULTS AND DISCUSSION

Synthesis of 6,6′- and 5,5′-Substituted Isoindigo Derivatives. The syntheses of 6,6′- and 5,5′-substituted isoindigo derivatives are summarized in Scheme 1. The dibromo species, **6,6′-Br**, was synthesized via procedures from the literature.[13] The precursor, **5,5′-H** (Supporting Information), was obtained via an adapted procedure involving acid-catalyzed adol condensation and dehydration between 5-bromoisatin and 5-bromooxindile. Alkylation of **5,5′-H** further gave us the ethylhexyl substituted **5,5′-Br**.

6,6′-BT was obtained by Suzuki coupling reaction between Benzo[b]thien-2-ylboronic acid and **6,6′-Br** in the presence of tris(dibenzylideneacetone)-dipalladium, $Pd_2(dba)_3$, as well as $[(^tBu)_3PH]BF_4$ and K_3PO_4 in THF/H_2O. For **6,6′-BZ**, Stille coupling reaction between **6,6′-Br** and stannyl benzothizole in the presence of tetrakis(triphenylphosphine)-palladium, $Pd[P(Ph)_3]_4$ in toluene was carried out. In the Stille coupling reaction between **5,5′-Br** and stannyl benzothizole, we obtained only the monosubstituted product when $Pd(PPh_3)_4$ was used as the catalyst in toluene under reflux conditions, likely due to low reactivity of bromine at the 5,5′-positions of the isoindigo core. In the presence of tris(dibenzylideneacetone)-dipalladium, $Pd_2(dba)_3$, as well as $[(^tBu)_3PH]BF_4$ and CsF in toluene, however, we were able to obtain the disubstituted benzothizole derivative, **5,5′-BZ,** under reflux condition. With this optimized protocol, the 5,5′-substituted benzothiophene derivative, **5,5′-BT**, was obtain using $Pd_2(dba)_3$, $[(^tBu)_3PH]BF_4$ and K_3PO_4 as base in a THF and water mixture under reflux condition. All compounds were characterized by ^1H, ^{13}C NMR spectroscopy, and high-resolution mass spectrometry, the data of which are provided in the Supporting Information.

Effects of 6,6′- and 5,5′-Substitution on the Photophysical Properties of Isoindigo Derivatives. The photophysical properties of the dibromo isoindigo precursors are discussed in detail in Supporting Information. Similar to the absorbance spectra of the dibromo precursors, we see distinctive differences between the spectra of the 6,6′- and 5,5′-substituted isoindigo compounds. The UV−vis spectra of the new isoindigo derivatives are shown in Figure 1. The photophysical data are also summarized in Table 1. Similar to the UV−vis spectra of the **6,6′-Br**, the UV−vis spectra of the 6,6′-substituted compounds generally exhibit stronger CT bands in the visible compared to those of the 5,5′-substituted compounds. At 2600 L mol^{-1} cm^{-1} and 1800 L mol^{-1} cm^{-1}, the molar extinction coefficients of **5,5′-BT** and **5,5′-BZ** are at least an order of magnitude lower than those of the 6,6′-substituted counterparts, with **6,6′-BT**'s molar extinction coefficient at 40 300 L mol^{-1} cm^{-1} and that of **6,6′-BZ** at 17 500 L mol^{-1} cm^{-1} in solution. The large disparity in the molar extinction coefficients suggests stronger electronic coupling between the terminal groups and the isoindigo core in the 6,6′-, as opposed to the 5,5′-substituted, compounds. This hypothesis is further supported by our theoretical studies that electronic coupling between the ground state and the excited state is stronger in 6,6′-derivatives (see details in theoretical section).[30] Compared to 6,6′- and 5,5′-carbazole-based donor−acceptor

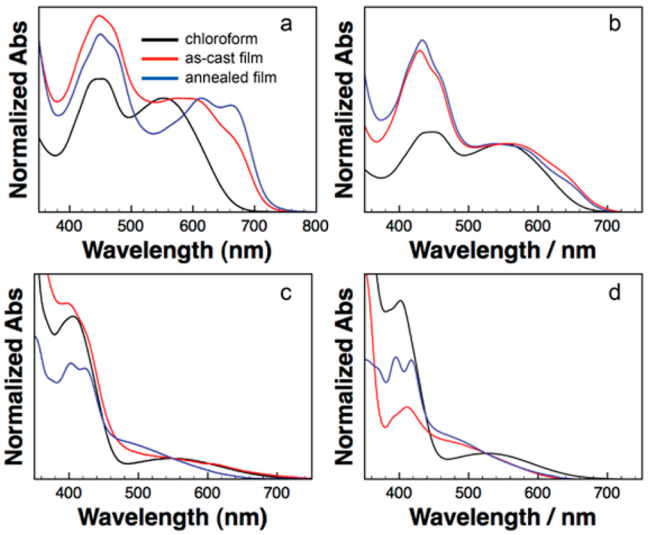

Figure 1. UV–vis spectra of (a) **6,6′-BT**, (b) **6,6′-BZ**, (c) **5,5′-BT**, (d) **5,5′-BZ**.

polymeric systems in the literature, such pronounced difference in absorptivity could be due to differences in the electronic structure of the isoindigo-based donor–acceptor systems.[31]

In Figure 1a, we observe that the λ_{max} of the CT band of **6,6′-BT** red-shifts from 553 nm in the solution spectrum to 597 nm in the solid-state spectrum. We attribute this red shift to an increase in conjugation due to planarization of the backbone and increased intermolecular $\pi-\pi$ interaction in the solid state. Upon solidification, we also observe the emergence of a vibronic shoulder between 650 and 700 nm. This vibronic shoulder grows in absorbance as the film is subjected to thermal annealing at 120 °C for 10 min. Like the UV–vis spectra of poly(3-hexyl thiophene), P3HT,[32−35] the emergence and subsequent growth of a vibronic peak at 660 and 614 nm is correlated with enhanced solid-state crystallinity and ordering of **6,6′-BT**, first upon solidification, and then upon thermal annealing.

The UV–vis spectra of **6,6′-BZ** with electron-poor benzothiazole substituent are provided in Figure 1b. In contrast with the UV–vis spectra of **6,6′-BT**, the CT band of **6,6′-BZ** does not red shift substantially on solidification; we only observe a $\Delta\lambda_{max}$ of 5 nm between the λ_{max} extracted from the solution spectrum and that extracted from the as-cast thin film spectrum. Although we observe the emergence of a weak vibronic shoulder upon solidification, thermal annealing does little to increase the absorbance of this vibronic shoulder. We believe this marked difference in the evolution of the solid-state UV–vis spectra between **6,6′-BT** and **6,6′-BZ** can be attributed to differences in the solid-state organization as a result of the intermolecular donor–acceptor interactions between the substituent and the isoindigo core. **BT** is electron-rich and can couple strongly to the electron poor isoindigo core of adjacent molecules, resulting in head-to-tail type *J*-aggregation, whereas **BZ** is electron poor and cannot maintain strong intermolecular donor–acceptor interactions with the isoindigo core on neighboring molecules. As a consequence, attachment of **BZ** to **6,6′-Br** has limited influence on its solid-state optical spectra.

Compared to the 6,6′-substituted isoindigo derivatives, the 5,5′-substituted compounds exhibit characteristically different absorption spectra both in solution and in their solid states. The UV–vis spectra of **5,5′-BT** and **5,5′-BZ** are provided in panels c and d in Figure 1, respectively. These spectra exhibit weak CT bands and they look qualitatively similar to those of **5,5′-Br**. On the basis of theoretical studies (see section below), the substantially weaker CT band in the **5,5′**-derivatives could stem from stronger charge separation since the electronic coupling between the substituent and the isoindigo core is weak when substitution occurs at the 5,5′-positions.[30] We note, however, an important difference between the solution absorbance spectra of **5,5′-BT** and **5,5′-BZ**. The λ_{max} extracted from the solution spectrum of **5,5′-BZ** at 525 nm is smaller compared to the λ_{max} of 550 nm of the solution spectrum of **5,5′-BT**. In fact, the λ_{max} extracted from the solution spectrum of **5,5′-BZ** is comparable to that of **5,5′-Br**. Given that there is limited electronic communication between the substituent and the isoindigo core in the 5,5′-substituted compounds, this observation further implies that the energy of the CT bands of these compounds depends on the electronic nature of the substitution, with the more electron rich **BT** substitution lowering the energy of the CT band more effectively. In contrast, the stronger electronic coupling between the substituent at the 6,6′-positions and the isoindigo core plays a more dominant role so the CT band energies are not solely dependent on the electronic nature of the substitution. Compared to their solution spectra, the UV–vis spectra acquired in the solid state of **5,5′-BT** and **5,5′-BZ** exhibit blue-shifted absorption shoulders between 500–600 nm and enhanced absorbances in the 450–500 nm range, suggesting the formation of *H*-aggregates on solidification of the 5,5′-substituted isoindigo derivatives.[36] This observation is very different from that previously reported on carbazole-based donor–acceptor polymers where the solid-state spectra of both 6,6′- and 5,5′-substituted polymers are similar and only showed a 20 nm red-shift in λ_{max} relative to their solution spectra, suggesting comparably weak solid-state organization in carbazole polymers irrespective of substituent placement.[31]

A comparison of the UV–vis spectra of the four isoindigo compounds under study reveals that both the chemical nature of the substituent and the placement of the substituent are important in influencing the electronic structure and molecular

Table 1. Experimental and Theoretical Values of Energy Levels of 6,6′- and 5,5′-Substituted Isoindigo Derivatives

compd	λ_{max}[a] (nm)	ε[b]	E_{opt}[c] (eV)	HOMO[d] (eV)	LUMO[e] (eV)	HOMO[f] (eV)	LUMO[f] (eV)
6,6′-BT	553 (539)	40 300	1.70	−5.44	−3.74	−5.35	−2.86
6,6′-BZ	550 (535)	17 500	1.76	−5.75	−3.99	−5.59	−3.04
5,5′-BT	549 (535)	1800	1.96	−5.64	−3.68	−5.34	−2.86
5,5′-BZ	525 (520)	2600	2.03	−5.53	−3.50	−5.59	−2.99

[a]Measured in $CHCl_3$, measured in cyclohexane in parentheses. [b]Molar extinction coefficient (L mol^{-1} cm^{-1}). [c]Obtained from onset absorption of thermally annealed thin films. [d]Determined by photoelectron spectrometer (AC-2) at ambient conditions. [e]$E_{LUMO} = E_{opt} - |E_{HOMO}|$. [f]TD-DFT calculated at theoretical level of TD-B3LYP/6-31G(d).

organization of these new isoindigo model compounds. 6,6′-substitution on the isoindigo core promotes stronger electronic coupling with its chemical substitution leading to stronger photoabsorptivity. In the solid state, 6,6′-substitution also promotes *J*-aggregation in the solid state, particularly when the substituent is electron-rich **BT**. Interestingly, the UV−vis spectrum of an isoindigo derivative having benzofuran, **BF**, as the substituent at the 6,6′-positions only exhibits a small red shift in its solid-state absorption compared to that in solution.[21] That **BF** is also electron-rich, yet the authors did not observe a marked red shift in its absorption upon solidification, which points to the uniqueness of **BT** substituent in supporting head-to-tail *J*-aggregation in the solid state.

Theoretical Studies of 6,6′- And 5,5′-Substitution of Isoindigo Derivatives. Density functional theory (DFT) and time-dependent DFT calculations were carried out at the B3LYP/6-31G(d) level of theory[28] to further reveal the electronic effects of 6,6′- and 5,5′-substitution on the isoindigo derivatives. In order to reduce computation time, the ethylhexyl solubilizing side chain was replaced with a methyl substituent for these calculations. As such, these compounds are labeled **6,6′-BT′/BZ′** and **5,5′-BT′/BZ′**, with the apostrophe to signify this change in the alkyl chain substitution. Figure 2 shows the

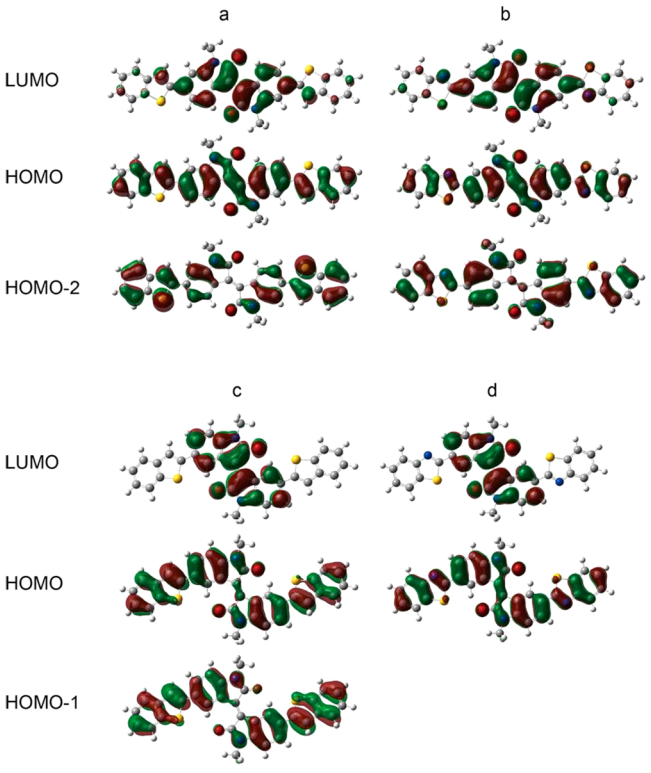

Figure 2. Frontier molecular orbitals of (a) **6,6′-BT′**, (b) **6,6′-BZ′**, (c) **5,5′-BT′**, (d) **5,5′-BZ′**.

results of these calculations, with the molecular orbitals depicted graphically. The HOMO and LUMO energy levels extracted from this exercise are summarized in Table 1. Our calculations show that the lowest transition of **6,6′-BT′** and **6,6′-BZ′** mainly involves HOMO ⇒ LUMO and HOMO−2 ⇒ LUMO transitions with weights of 94.5% and 3.1% for **6,6′-BT′** and 91.8% and 7.1% for **6,6′-BZ′**, respectively. We observe delocalization of the electron density distribution in the HOMO across the entire molecule for both **6,6′-BT′** and **6,6′-BZ′**. The electron density distribution in the LUMO is mostly concentrated on the isoindigo core, though we observe some electron density distribution from **BT** and **BZ** substituents in the LUMO. We also observe an electron density redistribution from the substituents to the isoindigo core involving HOMO−2 ⇒ LUMO, although this transition only contributes 3.1% of the S_0-S_1 transition. These observations suggest intramolecular charge transfer between 6,6′-substituted benzothiophene or benzothiazole and the isoindigo core occurring by an S_0−S_1 transition, with **6,6′-BT′** and **6,6′-BZ′** exhibiting similar predicted λ_{max} at 569 and 566 nm, respectively. These values are consistent with the λ_{max} extracted experimentally from the UV−vis spectra of **6,6′-BT** and **6,6′-BZ** in $CHCl_3$ in Figure 1.

The situation becomes more complicated with the 5,5′-substituted derivatives. For **5,5′-BT′**, the S_0−S_1 transition mainly involves HOMO ⇒ LUMO and HOMO−1 ⇒ LUMO with weights of 94.6% and 3.5% contribution, respectively. We found that HOMO and HOMO−1 are actually degenerate with energy levels at −5.61 eV and −5.68 eV, respectively. Compared to the 6,6′-substituted derivatives, the electron density distribution in the LUMO of **5,5′-BT′** is also markedly different. Specifically, the electron density distribution in the LUMO of **5,5′-BT′** appears to be localized on the isoindigo core without any contribution from the **BT** substitution at the 5,5′-positions. As such, we observe charge separation between the substituent and the isoindigo core that is consistent with our UV−vis experiments, further confirming weak coupling between the 5,5′-substituted **BT** and the isoindigo core.

Different from the other compounds under study, we found the S_0−S_1 transition of **5,5′-BZ′** mainly involve HOMO ⇒ LUMO with a weight of 97.2%. Consistent with UV−vis experiments, this S_0−S_1 transition energy of **5,5′-BZ′** at λ_{max} of 582 nm is much higher that that of **5,5′-BT′** at λ_{max} of 620 nm. We believe that such a difference can be correlated to the differences in the electron distribution between the HOMO of **5,5′-BZ′** and the HOMO and HOMO−1 of **5,5′-BT′** as the S_0-S_1 transition of **5,5′-BZ′** involving HOMO ⇒ LUMO induces a less pronounced charge separation state than that of **5,5′-BT′**. Therefore, the addition of a benzothiazole substitutent at the 5,5′-positions of the isoindigo core does not alter λ_{max} substantially.

These theoretical studies have also helped us to understand the effects of substituent placement on the intensity of the absorption transitions. Generally, the probability of an absorption transition is highly dependent on the electronic coupling between the ground and excited states of the molecule.[30] In donor−acceptor systems, an overlap of the frontier MOs results in a dipole moment of the optical transition from the ground state to the CT states, which manifests itself as a distinct CT absorption band in the optical spectra. Our calculations reveal that when the substituent is at the 6,6′-positions, it contributes to both the HOMO and LUMO orbitals, suggesting strong electronic coupling between the substituents and the isoindigo core. When the substituent is place at the 5,5′-positions, however, its addition contributes only to the LUMO orbital. Because HOMO−LUMO contributes ca. 90% of the S_0−S_1 transition, the stronger electronic coupling between substituents at the 6,6′-positions and the isoindigo core is likely responsible for the stronger absorptivity in these derivatives. Indeed, the calculated oscillator strengths for **5,5′-BT′** and **5,5′-BZ′** are 0.025 and 0.039; both lower than 0.86 of **6,6′-BT′** and 0.65 of **6,6′-BZ′**.

This difference is in line with the lower molar extinction coefficient of 5,5′-substituted compounds compared to the 6,6′-substituted derivatives.

The HOMO and LUMO energy levels were also obtained from DFT calculations provided in Table S1 in the Supporting Information. **6,6′-BZ′** and **5,5′-BZ′** with electron withdrawing benzothiazole substitution exhibit lower LUMO energy levels at −3.04 and −2.99 eV, respectively, compared to those of **6,6′-BT′** and **5,5′-BT′**, both at −2.86 eV. We also observed a similar trend for the HOMO energy levels of these materials. **5,5′-BZ′** and **5,5′-BZ′** with electron withdrawing benzothiazole substitution exhibit lower HOMO energy levels compared to the benzothiophene-substituted counterparts. These observations are consistent with the experimental HOMO and LUMO energy levels obtained by cyclic voltammetry and UV-via experiments listed inTable S1 in the Supporting Information.[37]

6,6′- and 5,5′-Substitution Effects on the HOMO and LUMO Energy Levels of Isoindigo Derivatives in the Solid State. Because the CV experiments were conducted on isoindigo derivatives dissolved in $CHCl_3$, the LUMO energy levels extracted from these experiments are characteristic of the compounds' molecular properties. Yet, the energy levels in the solid state are more relevant for device optimization. We thus estimated the HOMO and LUMO energy levels of the four compounds under study from solid-state experiments as well. These values will necessarily be different from those extracted from CV experiments as the solid-state experiments should account for changes to the energy levels induced by the presence of intermolecular interactions.[38] On the basis of the onset of absorption in the UV−vis spectra of thermally annealed thin films, we estimated **6,6′-BT** and **6,6′-BZ** to exhibit optical bandgaps of 1.70 and 1.76 eV, respectively. These values are smaller than those of **5,5′-BT** and **5,5′-BZ**, estimated at 1.96 and 2.02 eV, respectively. We independently determined the HOMO energy levels of the isoindigo derivatives in the solid state by photoelectron spectroscopy at ambient conditions; the results of which are summarized in Table 1. Of the four compounds tested, **6,6′-BZ** exhibits the highest HOMO energy level, at −5.75 eV. **6,6′-BT** exhibits a HOMO energy level of −5.44 eV, whereas **5,5′-BT** and **5,5′-BZ** exhibit HOMO energy levels of −5.64 and −5.53 eV, respectively.

As an electron donor candidate for solar cells, the higher HOMO energy level of **6,6′-BZ** compared to those of the other compounds could potentially lead to a higher open-circuit voltage in devices paired with $PC_{71}BM$.[39] Importantly, the energy offset between the LUMO energy levels of the electron donor and the electron acceptor, ΔE_{LUMO}, needs to be around 0.3−0.5 eV at the donor−acceptor interface to overcome the exciton binding energy for charge dissociation in OPVs.[40] Given the optical bandgap and the HOMO energy level estimated from photoelectron spectroscopy, we estimated the LUMO energy level of **6,6′-BT** in the solid state to be −3.74 eV away from vacuum; **6,6′-BZ**, **5,5′-BT** and **5,5′-BZ** exhibit LUMO energy levels that are −3.99, −3.68, and −3.50 eV away from vacuum in the solid state. We recognize that this exercise does not account for vacuum level misalignment and the presence of any interfacial dipoles, both of which can cause the energy levels to shift.[41] Nonetheless, such estimates of the energy levels of the neat constituents in the solid state provide a first-order analysis of whether these compounds can be suitably paired with $PC_{71}BM$ in solar cells. Assuming a LUMO energy level of −4.0 eV for $PC_{71}BM$,[42] ΔE_{LUMO} is estimated to be 0.56 and 0.31 eV when **6,6′-BT** and **6,6′-BZ** paired with $PC_{71}BM$. Similarly, we estimated ΔE_{LUMO} = 0.62 for **5,5′-BT** and ΔE_{LUMO} = 0.80 for **5,5′-BZ** when these compounds are in turn paired with $PC_{71}BM$. Given that ΔE_{LUMO} are either within or exceed the prescribed 0.3−0.5 eV required to overcome the exciton binding energy[40] when any of our isoindigo compounds are paired with $PC_{71}BM$, our compounds should promote efficient exciton dissociation and charge transfer in solar cells upon photoabsorption.

6,6′- and 5,5′-Substitution Effects on Molecular Organization of Isoindigo Derivatives. To understand the substitution effects on the molecular organization of these isoindigo derivatives in the solid state, we carried out GIXD experiments on thin films of these materials. X-ray diffraction traces of these molecules obtained by azimuthally integrating GIXD images are provided in Figure S4 in the Supporting Information. As shown in Figure S4a in the Supporting Information, the X-ray traces of as-cast films of 6,6′- and 5,5′-substituted isoindigo derivatives show a primary reflection at 0.42 $Å^{-1}$ for **6,6′-BT** and **5,5′-BT**, and at 0.41 $Å^{-1}$ for **6,6′-BZ**. A very weak primary reflection at 0.41 $Å^{-1}$ is observed in the X-ray trace of **5,5′-BZ**. Given that the X-ray diffraction patterns have all been normalized to account for thickness variations across the samples, variations in intensity to first order reflect differences in the crystallinity in these films. That the primary reflection in the X-ray trace of as-cast **5,5′-BZ** is the least intense suggests that it is the least crystalline among the films examined.

The GIXD images of the thermally annealed isoindigo derivatives thin films are shown in Figure 3. The azimuthally

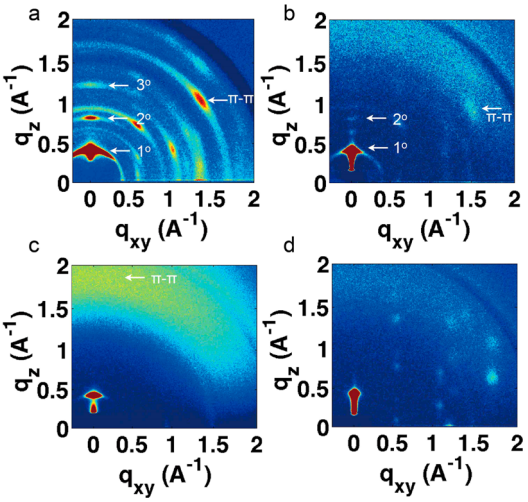

Figure 3. GIXD images of thermally annealed thin films of (a) **6,6′-BT**, (b) **6,6′-BZ**, (c) **5,5′-BT**, (d) **5,5′-BZ**.

integrated X-ray diffraction traces stemming from these images are provided in Figure S4b in the Supporting Information. The primary reflection in the XRD patterns of these compounds uniformly increases in intensity with thermal annealing (see Figure S4 in the Supporting Information); this observation suggests increases in crystallinities upon thermal annealing. This comparison also suggests that the **6,6′-BT** film is the most crystalline on thermal annealing. Returning to Figures 3a and b, we observe that the GIXD patterns of thermally annealed **6,6′-BT** and **6,6′-BZ** exhibit multiple higher-order reflections in the low-q region along the meridian suggesting the presence of

periodic lamellar structures in the out-of-plane direction. Compared to **6,6′-BZ**, **6,6′-BT** exhibits stronger higher-order reflections, suggesting that it is more ordered and more crystalline. From the placement of the first-order reflections, we estimate that the lamellar structures of both **6,6′-BT** and **6,6′-BZ** have identical periodic spacings of 14.9 Å. We hypothesize that the packing of **6,6′-BT** in the solid-state is similar to that of most conjugated oligomers and polymers having alkyl side chains.[43,44] This interlamellar spacing should thus correspond to the periodic distance between layers of alkyl chains. Convention wisdom has the addition of ethylhexyl side chain, as opposed to a linear alkyl side chain, interrupting intermolecular packing, such as in P3HT.[45−47] We thus believe that another intermolecular interaction, very likely $\pi-\pi$ stacking between the conjugated backbones instead of alkyl side chains, must play a more important role to facilitate solid-state lamellar formation in our isoindigo derivatives. Particularly, our result indicates that the electron-rich **BT** substituent is more influential than the electron-poor **BZ** substituent in inducing long-range lamellar ordering in the solid state of the 6,6′-substituted isoindigo compounds. Additionally, we observe a strong reflection at q of 1.7 $Å^{-1}$ in the GIXD image of **6,6′-BT**, corresponding to a characteristic spacing of 3.7 Å; we have accordingly attributed this reflection to the periodic $\pi-\pi$ distance of adjacent molecules. That this reflection appears 53° away from the meridian indicates that the π-stacking direction is tilted away from the substrate normal. For **6,6′-BZ**, a weak reflection is observed at q of 1.8 $Å^{-1}$ in its GIXD image, also suggesting the presence of $\pi-\pi$ interactions.

Compared to the GIXD patterns of **6,6′-BT** and **6,6′-BZ**, the GIXD patterns of the 5,5′- substituted derivatives shown in images c and d in Figure 3 reveal an absence of lamellar ordering in the solid state. We believe this difference in molecular organization stems from differences in the molecular geometry. While 6,6′-substituted isoindigo derivatives are linear, the 5,5′-substituted compounds are not, making it more difficult for these compounds to spontaneously self-assemble in the solid state. We do, however, observe a slight intensity enhancement at 1.7 $Å^{-1}$ along the meridian in the GIXD image of **5,5′-BT**, which we have attributed to weak intermolecular donor−acceptor interactions between the electron-rich **BT** substituent and the electron-poor isoindigo core on a neighboring molecule. Such structural differences between the 6,6′- and the 5,5′-substituted isoindigo compounds also manifest themselves in the AFM micrographs shown in Figure 4. In Figure 4a, we observe large 2D structures in the annealed **6,6′-BT** film, consistent with those of molecules having head-to-tail type stacking in the solid state.[36] This 2D growth habit is absent from the thin films of the other derivatives.

6,6′- and 5,5′-Substitution Effects on Device Characteristics of Solar Cells Comprising Isoindigo Derivatives. The isoindigo-based compounds under study were incorporated into bulk-heterojunction solar cells as electron donors with $PC_{71}BM$ as the electron acceptor. Initially, all new isoindigo derivatives were blended with $PC_{71}BM$ at a 1:1 mass ratio to screen for the most promising donor material. The characteristics of such devices are summarized in Table 2 and Table S2 in the Supporting Information. In general, devices comprising these isoindigo derivatives exhibit disappointingly low power-conversion efficiencies, PCEs (approximately 0.01%) with the exception of devices comprising **6,6′-BT** and $PC_{71}BM$, which exhibit an average PCE of 0.47 ± 0.05% after

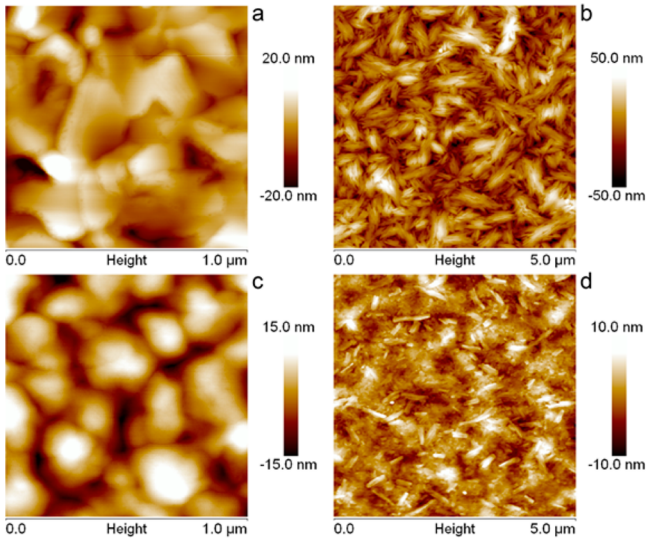

Figure 4. AFM images of thermally annealed thin films of (a) **6,6′-BT**, (b) **6,6′-BZ**, (c) **5,5′-BT**, (d) **5,5′-BZ**.

Table 2. Device Performance of Solar Cells Having Isoindigo Derivatives and $PC_{71}BM$ at a Blend Ratio of 50:50 by Mass[a]

compd[b]	V_{oc} (V)	J_{sc} (mA/cm²)	FF (%)	PCE (%)
6,6′-BT	0.66 ± 0.02	2.02 ± 0.2	35 ± 0.7	0.47 ± 0.05
6,6′-BZ	0.40 ± 0.03	0.08 ± 0.02	29 ± 1.0	0.01 ± 0.003
5,5′-BT	0.48 ± 0.04	0.08 ± 0.007	32 ± 1.0	0.01 ± 0.002
5,5′-BZ	0.48 ± 0.04	0.08 ± 0.007	32 ± 1.0	0.01 ± 0.02

[a]Device performance after thermal annealing at 120 °C for 10 min and on the basis of 4−5 devices tested. [b]20 mg/mL in $CHCl_3$, spin-coated at 1500 rpm for 20 s.

thermal annealing. Several reasons could contribute to **6,6′-BT** making a better donor candidate compared to the other isoindigo compounds. First, **6,6′-BT** blend exhibits the strongest and broadest solid-state light absorption among all the isoindigo compounds under study that can be attributed to strong J-aggregation induced low energy absorption (see Figure S5a in the Supporting Information). The external quantum efficiency trace shown inFigure S5b in the Supporting Information substantiates that a significant contribution of photocurrent generation does indeed arise from photo-absorption between 600 and 700 nm of **6,6′-BT** in *J*-aggregation. The open-circuit voltage, V_{oc}, of devices comprising **6,6′-BT** and $PC_{71}BM$ is higher compared to those containing the other isoindigo derivatives. This observation, however, is not consistent with the measured HOMO energy levels in the solid state, likely because the energy levels of the neat constituents do not account for interfacial dipoles and vacuum level misalignment that may be present in the blend.[41] Importantly, the solid-state morphology has also been reported to affect the V_{oc}, as it too can affect charge recombination in the active layer.[48] Both hole and electron mobilities of the photoactive blends were determined from space charge limited current (SCLC) measurements.[49−51] The hole mobilities of our isoindigo derivatives are uniformly an order of magnitude lower than their corresponding electron mobilities; this observation is consistent with our observation that our devices uniformly having low fill factors, FFs. Given that **6,6′-BT** containing devices exhibit the highest solar cell

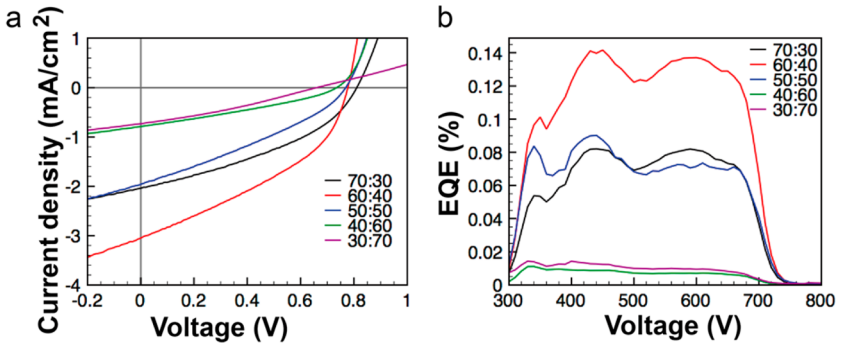

Figure 5. Device characteristics of organic solar cells comprising photoactive blends of **6,6′-BT** and $PC_{71}BM$ at different mass ratios.

performance despite the fact that these same photoactive layers do not show the highest hole mobility, we suspect that its stronger solid-state absorption and more organized solid-state structure dominate charge generation and transport.

Given the initial success with **6,6′-BT**, we further optimized the processing conditions of active layers of **6,6′-BT** and $PC_{71}BM$ to increase device performance. Figure 5 shows the *J*–*V* characteristics and the external quantum efficiency spectra, EQE, of organic solar cells having active layers of **6,6′-BT** and $PC_{71}BM$ at different mass ratios after thermal annealing; the extracted device parameters are provided in Table 3. Increasing

Table 3. Device Performance of Solar Cells Having Bulk-Heterojunction Active Layers of 6,6′-BT and $PC_{71}BM$ at Different Blend Ratios[a]

blend ratio[b]	V_{oc} (V)	J_{sc} (mA/cm^2)	FF (%)	PCE (%)
30:70	0.65 ± 0.02	0.67 ± 0.04	31 ± 0.0	0.13 ± 0.01
40:60	0.65 ± 0.01	0.69 ± 0.05	36 ± 0.5	0.16 ± 0.01
50:50	0.66 ± 0.02	2.02 ± 0.18	35 ± 0.7	0.47 ± 0.05
60:40	0.78 ± 0.01	2.92 ± 0.20	38 ± 0.3	0.87 ± 0.04
60:40[c]	0.78 ± 0.02	4.11 ± 0.71	37 ± 1.1	1.19 ± 0.21
70:30	0.80 ± 0.01	1.94 ± 0.09	38 ± 0.3	0.59 ± 0.03

[a]Device performance on the basis of 4–5 devices tested. [b]20 mg/mL in $CHCl_3$, spin-coated at 1500 rpm for 20 s; active layer thermally annealed at 120 °C for 10 min. [c]With PDMS (M.W. = 14 000 g/mol) at 0.1 mg/mL of solution.

6,6′-BT fraction increases the performance of devices. In particular, the average V_{oc} increases from 0.65 ± 0.02 V for solar cells having 30:70 **6,6′-BT**:$PC_{71}BM$ active layers to 0.80 ± 0.01 V for devices having 70:30 **6,6′-BT**:$PC_{71}BM$ active layers. Such composition-dependent variation in V_{oc} had previously been seen in P3HT:$PC_{61}BM$ devices.[52,53] The average short-circuit current, J_{sc}, increases with increasing fraction of **6,6′-BT** as well, with the highest J_{sc} recorded for devices having an active layer of 60:40 **6,6′-BT**:$PC_{71}BM$. Cumulatively, we found devices having active layers with 60:40 **6,6′-BT**:$PC_{71}BM$ to exhibit the highest PCE. These devices exhibit an average J_{sc} of 2.92 ± 0.20 mA/cm^2, an average V_{oc} of 0.78 ± 0.01 V, and an average FF of 38 ± 0.3%, resulting in an average PCE of 0.87 ± 0.04%. We also observe that the hole mobilities increase upon increasing the donor fraction leading to more balanced hole and electron mobilities (see Table S3 in the Supporting Information). Although we observe an increase in FF with increasing donor ratio in the bulk-heterojunction active layers, the FFs of our best devices remain lower than 40%, which we have tentatively attributed to the imbalance in electron and hole mobilities that remain, even in optimized devices.

Although our devices show 3 times higher PCE over bulk-heterojunction devices previously reported with a 6,6′-benzofuran-substituted isoindigo derivative,[21] the device characteristics remain low compared to record efficiencies reported for organic solar cells comprising molecular semiconductors. Given the respectable V_{oc}, that the PCE is not higher in these devices is attributed to the low J_{sc} and FF and is suggestive of the presence of a substantial space charge recombination zone. To further optimize device performance, we used polydimethylsiloxane, PDMS,[14,16] having a molecular weight of 14 000 g/mol, as an additive in the active layers of 60:40 **6,6′-BT** and $PC_{71}BM$. Upon the addition of 0.1 mg/mL of PDMS, the performance of **6,6′-BT** and $PC_{71}BM$ bulk-heterojunction solar cells was further improved to an average J_{sc} as high as 4.11 ± 0.71 mA/cm^2. The average V_{oc} and FF remain unchanged, resulting in an average PCE of 1.19 ± 0.21%. The best device in the presence of PDMS exhibits an efficiency of 1.4% and a J_{sc} of 4.9 mA/cm^2.

CONCLUSIONS

A series of 6,6′- and 5,5′-substituted isoindigo model compounds were synthesized to elucidate the effects of the electronic nature of the substituent and its placement on the photophysical/redox properties and solid-state organization. As the first systematic study of isoindigo-based small molecules, our studies show that both the placement and the electronic nature of the substituent play important roles on the molecular properties and corresponding device performance of OPVs containing these materials. Generally, 6,6′-substitution enhances the presence of a low energy charge-transfer band due to stronger electronic communication between the substituent and the isoindigo core; while a weaker CT band can be observed in the 5,5′-substituted derivatives. In the solid state, 6,6′-substitution of isoindigo derivatives induces *J*-aggregation and well-organized lamellar structures in the solid state, whereas 5,5′-substitution of isoindigo derivatives induces *H*-aggregation in the solid state. Particularly, benzothiophene substitution at the 6,6′-positions of isoindigo induces strong intermolecular donor–acceptor interactions between electron-rich benzothiophene substituents and electron-poor isoindigo cores on adjacent molecules. Because of the higher absorptivity and well-organized solid-state structure, the incorporation of **6,6′-BT** in solar cells thus resulted in higher device performance as electron donor, compared to the other isoindigo derivatives under study.

■ ASSOCIATED CONTENT

Supporting Information

Details of synthetic procedures, CV data, GIXD images, UV−vis absorption data, and theoretical calculation data. This material is available free of charge via the Internet at http://pubs.acs.org.

■ AUTHOR INFORMATION

Corresponding Author

*E-mail: lloo@princeton.edu. Tel: +1 609-258-9091.

Notes

The authors declare no competing financial interest.

■ ACKNOWLEDGMENTS

This work was supported by ONR's Photovoltaic Program (N00014-11-10328) and NSF-sponsored MRSEC through the Princeton Center for Complex Materials (Grant DMR-0819860), which also provided access to the PRISM Imaging and Analysis Center. GIXD experiments were conducted at CHESS, which is supported by NSF and NIH/NIGMS under award DMR-0936384. Y.R. thanks PCCM-MRSEC for a postdoctoral fellowship. A.M.H is supported on an NDSEG graduate fellowship while L.W.-B. is supported on a L'Oreal Women in Science postdoctoral fellowship.

■ REFERENCES

(1) Chen, Y.; Wan, X.; Long, G. High Performance Photovoltaic Applications Using Solution-Processed Small Molecules. *Acc. Chem. Res.* **2013**, *46*, 2645−2655.

(2) Mishra, A.; Bäuerle, P. Small Molecule Organic Semiconductors on the Move: Promises for Future Solar Energy Technology. *Angew. Chem., Int. Ed.* **2012**, *51*, 2020−2067.

(3) Lin, Y.; Li, Y.; Zhan, X. Small Molecule Semiconductors for High-Efficiency Organic Photovoltaics. *Chem. Soc. Rev.* **2012**, *41*, 4245−4272.

(4) Zhang, Z.-G.; Wang, J. Structure and Properties of Conjugated Donor-Acceptor Copolymers for Solar Cell Applications. *J. Mater. Chem.* **2012**, *22*, 4178−4187.

(5) Henson, Z. B.; Müllen, K.; Bazan, G. C. Design Strategies for Organic Semiconductors Beyond the Molecular Formula. *Nat. Chem.* **2012**, *4*, 699−704.

(6) Coughlin, J. E.; Henson, Z. B.; Welch, G. C.; Bazan, G. C. Design and Synthesis of Molecular Donors for Solution-Processed High-Efficiency Organic Solar Cells. *Acc. Chem. Res.* **2014**, *47*, 257−270.

(7) Qu, S.; Tian, H. Diketopyrrolopyrrole (DPP)-Based Materials for Organic Photovoltaics. *Chem. Commun.* **2012**, *48*, 3039−3051.

(8) Liu, J.; Walker, B.; Tamayo, A.; Zhang, Y.; Nguyen, T.-Q. Effects of Heteroatom Substitutions on the Crystal Structure, Film Formation, and Optoelectronic Properties of Diketopyrrolopyrrole-Based Materials. *Adv. Funct. Mater.* **2013**, *23*, 47−56.

(9) Walker, B.; Tamayo, A.; Dang, X.-D.; Zalar, P.; Seo, J. H.; Garcia, A.; Tantiwiwat, M.; Nguyen, T.-Q. Nanoscale Phase Separation and High Photovoltaic Efficiency in Solution-Processed, Small-Molecule Bulk Heterojunction Solar Cells. *Adv. Funct. Mater.* **2009**, *19*, 3063−3069.

(10) Shin, W.; Yakuda, T.; Watanabe, G.; Yang, Y. S.; Adachi, C. Self-Organizing Mesomorphic Diketopyrrolopyrrole Derivatives for Efficient Solution-Processed Organic Solar Cells. *Chem. Mater.* **2013**, *25*, 2549−2556.

(11) Tamayo, A. B.; Walker, B.; Nguyen, T.-Q. A Low Band Gap, Solution Processable Oligothiophene with a Diketopyrrolopyrrole Core for Use in Organic Solar Cells. *J. Phys. Chem. C* **2008**, *112*, 11545−11551.

(12) Takacs, C. J.; Sun, Y.; Welch, G. C.; Perez, L. A.; Liu, X.; Wen, W.; Bazan, G. C.; Heeger, A. J. Solar Cell Efficiency, Self-Assembly and Dipole-Dipole Interactions of Isomorphic Narrow-Band-Gap Molecules. *J. Am. Chem. Soc.* **2012**, *134*, 16597−16606.

(13) Mei, J.; Graham, K. R.; Stalder, R.; Reynolds, J. R. Synthesis of Isoindigo-Based Oligothiophenes for Molecular Bulk Heterojunction Solar Cells. *Org. Lett.* **2010**, *12*, 660−663.

(14) Graham, K. R.; Mei, J.; Stalder, R.; Shim, J. W.; Cheun, H.; Steffy, F.; So, F.; Kippelen, B.; Reynolds, J. R. Polydimethylsiloxane as a Macromolecular Additive for Enhanced Performance of Molecular Bulk Heterojuction Organic Solar Cells. *ACS Appl. Mater. Interfaces* **2011**, *3*, 1210−1215.

(15) Estrada, L. A.; Liu, D. Y.; Salazar, D. H.; Dyer, A. L.; Reynolds, J. R. Poly[Bis-EDOT-Isoindigo]: An Electroactive Polymer Applied to Electrochemical Supercapacitors. *Macromolecules* **2012**, *45*, 8211−8220.

(16) Graham, K. R.; Wieruszewski, P. M.; Stalder, R.; Hartel, M. J.; Mei, J.; So, F.; Reynolds, J. R. Improved Performance of Molecular Bulk-Heterojunction Photovoltaic Cells Through Predictable Selection of Solvent Additives. *Adv. Funct. Mater.* **2012**, *21*, 4801−4813.

(17) Estrada, L. A.; Stalder, R.; Abbound, K. A.; Risko, C.; Bréda, J.-L.; Reynods, J. R. Understanding the Electronic Structure of Isoindigo in Conjugated Systems: a Combined Theoretical and Experimental Approach. *Macromolecules* **2013**, *46*, 8832−8844.

(18) Wang, E.; Mammo, W.; Andersson, M. R. Isoindigo-Based Polymers and Small Molecules for Bulky Heterojunction Solar Cells and Field Effect Transistors. *Adv. Mater.* **2014**, *26*, 1801−1826.

(19) Stalder, M. R.; Mei, J.; Graham, K. R.; Estrada, L. A.; Reynolds, J. R. Isoindigo, A Versatile Electron-Deficient Unit For High-Performance Organic Electronics. *Chem. Mater.* **2014**, *26*, 664−678.

(20) Deng, Y.; Liu, J.; Wang, J.; Liu, L.; Li, W.; Tian, H.; Zhang, X.; Xie, Z.; Geng, Y.; Wang, F. Dithienocarbazole and Isoindigo Based Amorphous Low Bandgap Conjugated Polymers for Efficient Polymer Solar Cells. *Adv. Mater.* **2014**, *26*, 471−476.

(21) Yassin, A.; Leriche, P.; Allain, M.; Roncali, J. Donor-Acceptor-Donor (D-A-A) Molecules Based on Isoindigo as Active Material for Organic Solar Cells. *New J. Chem.* **2013**, *37*, 502−507.

(22) Liu, Q.; Du, Z.; Chen, W.; Sun, L.; Chen, Y.; Sun, M.; Yang, R. Low HOMO Isoindigo Based Small Molecule for High Open-circuit Voltage 1.0 V Solution Processed Organic Solar Cells. *Synth. Met.* **2013**, *178*, 38−43.

(23) Wang, T.; Chen, Y.; Bao, X.; Du, Z.; Guo, J.; Wang, N.; Sun, M.; Yang, R. A New Isoindigo-Based Molecule with Ideal Energy Levels for Solution-Processable Organic Solar Cells. *Dyes Pigm.* **2013**, *98*, 11−16.

(24) Yang, M.; Chen, X.; Zou, Y.; Pan, C.; Liu, B.; Zhong, H. A Solution-Processable D-A-D Small Molecule Based on Isoindigo for Organic Solar Cells. *J. Mater. Sci.* **2013**, *48*, 1014−1020.

(25) Elsawy, W.; Lee, C.-L.; Cho, S.; Oh, S.-H.; Moon, S.-H.; Elbarbary, A.; Lee, J.-S. Isoindigo-Based Small Molecules for High-Performance Solution-Processed Organic Photovoltaic Devices: the Electron Donating Effect of the Donor Group on Photo-Physical Properties and Device Performance. *Phys. Chem. Chem. Phys.* **2013**, *15*, 15193−15203.

(26) Luňák, S., Jr.; Horáková, P.; Lycka, A. Absorption and Fluorescence of Arylmethylidenoxindoles and Isoindigo. *Dyes Pigm.* **2010**, *85*, 171−176.

(27) Bialas, D.; Suraru, S.-L.; Schmidt, R.; Würther, F. Thiophene-Functionalized Isoindigo Dyes Bearing Electron Donor Substituents with Absorptions Approaching the Near Infrared Region. *Org. Biomol. Chem.* **2011**, *9*, 6127−6132.

(28) Frisch, M. J.; Trucks, G. W.; Schlegel, H. B.; Scuseria, G. E.; Robb, M. A.; Cheeseman, J. R.; Montgomery, J. A., Jr.; Vreven, T.; Kudin, K. N.; Burant, J. C.; Millam, J. M.; Iyengar, S. S.; Tomasi, J.; Barone, V.; Mennucci, B.; Cossi, M.; Scalmani, G.; Rega, N.; Petersson, G. A.; Nakatsuji, H.; Hada, M.; Ehara, M.; Toyota, K.; Fukuda, R.; Hasegawa, J.; Ishida, M.; Nakajima, T.; Honda, Y.; Kitao, O.; Nakai, H.; Klene, M.; Li, X.; Knox, J. E.; Hratchian, H. P.; Cross, J. B.; Bakken, V.; Adamo, C.; Jaramillo, J.; Gomperts, R.; Stratmann, R. E.; Yazyev, O.; Austin, A. J.; Cammi, R.; Pomelli, C.; Ochterski, J. W.; Ayala, P. Y.; Morokuma, K.; Voth, G. A.; Salvador, P.; Dannenberg, J.

J.; Zakrzewski, V. G.; Dapprich, S.; Daniels, A. D.; Strain, M. C.; Farkas, O.; Malick, D. K.; Rabuck, A. D.; Raghavachari, K.; Foresman, J. B.; Ortiz, J. V.; Cui, Q.; Baboul, A. G.; Clifford, S.; Cioslowski, J.; Stefanov, B. B.; Liu, G.; Liashenko, A.; Piskorz, P.; Komaromi, I.; Martin, R. L.; Fox, D. J.; Keith, T.; Al-Laham, M. A.; Peng, C. Y.; Nanayakkara, A.; Challacombe, M.; Gill, P. M. W.; Johnson, B.; Chen, W.; Wong, M. W.; Gonzalez, C.; Pople, J. A. *Gaussian 03*, Revision E. 01; Gaussian Inc.: Wallingford, CT, 2007.

(29) Hiszpanski, A. M.; Lee, S. S.; Wang, H.; Woll, A. R.; Nuckolls, C.; Loo, Y.-L. Post-Deposition Processing Methods to Induce Preferential Orientation in Contorted Hexabenzocoronene Thin Films. *ACS Nano* **2013**, *7*, 294−300.

(30) Vauthey, E. Photoinduced Symmetry-Breaking Charge Separation. *ChemPhysChem* **2012**, *13*, 2001−2011.

(31) Kim, J.; Kwon, Y. S.; Shin, W. S.; Moon, S.-J.; Park, T. Carbazole-Based Copolymers: Effects of Conjugated Breaks and Steric Hindrance. *Macromolecules* **2011**, *44*, 1909−1919.

(32) Agostinelli, T.; Lilliu, S.; Labram, J. G.; Campoy-Quiles, M.; Hampton, M.; Pires, E.; Rawle, J.; Bikondoa, O.; Bradley, D. C.; Anthopoulos, T. D.; Nelson, J.; Macdonald, J. E. Real-Time Investigation of Crystallization and Phase-Segregation Dynamics in P3HT:PCBM Solar Cells during Thermal Annealing. *Adv. Funct. Mater.* **2011**, *21*, 1701−1708.

(33) Verploegen, E.; Mondal, R.; Bettinger, C. J.; Sok, S.; Toney, M. F.; Bao, Z. Effect of Thermal Annealing upon the Morphology of Polymer-Fullerene Blends. *Adv. Funct. Mater.* **2010**, *20*, 3519−3529.

(34) Camaioni, N.; Ridolfl, G.; Casalbore-Miceli, G.; Possamai, G.; Maggini, M. The Effect of a Mild Thermal Treatment on the Performance of Poly(3-alkylthiophene)/Fullerene Solar Cells. *Adv. Mater.* **2002**, *14*, 1735−1738.

(35) Li, G.; Shrotriya, V.; Yao, Y.; Yang, Y. Investigation of Annealing Effects and Film Thickness Dependence of Polymer Solar Cells Based on Poly(3-hexylthiophene). *J. Appl. Phys.* **2005**, *98*, 43704.

(36) Gierschner, J.; Park, S. Y. Luminescent Distyrylbenzenes: Tailoring Molecular Structure and Crystalline Morphology. *J. Mater. Chem. C* **2013**, *1*, 5818−5832.

(37) The experimental LUMO energy levels were derived from the reduction potentials of the compounds provided in Figure S1 in the Supporting Information. The HOMO energy levels were then estimated on the basis of the experimental LUMO energy levels and the optical bandgap extracted as λ_{onset} from the solution UV−vis spectra.

(38) Cornil, J.; Beljonne, D.; Calbert, J.-P.; Brédas, J.-L. Interchain Interactions in Organic π-Conjugated Materials: Impact on Electronic Structure, Optical Response, and Charge Transport. *Adv. Mater.* **2001**, *13*, 1053−1067.

(39) Qi, B.; Wang, J. Open-Circuit Voltage in Organic Solar Cells. *J. Mater. Chem.* **2012**, *22*, 24315−24325.

(40) Li, Y. Molecular Design of Photovoltaic Materials for Polymer Solar Cells: toward Suitable Electronic Energy Levels and Broad Absorption. *Acc. Chem. Res.* **2012**, *45*, 723−733.

(41) Guan, Z.-L.; Kim, J. B.; Wang, H.; Jaye, C.; Fisher, D. A.; Loo, Y.-L.; Kahn, A. Direct Determination of the Electronic Structure of the Poly(3-hexylthiophene):Phenyl-[6,6]-C61 Butyric Acid Methyl Ester Blend. *Org. Electron.* **2010**, *11*, 1779−1785.

(42) Kang, S. J.; Ahn, S.; Kim, J. B.; Schenck, C.; Hiszpanski, A. M.; Oh, S.; Schiros, T.; Loo, Y.-L.; Nuckolls, C. Using Self-Organization to Control Morphology in Molecular Photovoltaic. *J. Am. Chem. Soc.* **2013**, *135*, 2207−2212.

(43) Chen, T.-A.; Wu, X.; Rieke, R. D. Regiocontrolled Synthesis of Poly(3-alkylthiophene) Mediated by Rieke Zinc: Their Characterization and Solid-State Properties. *J. Am. Chem. Soc.* **1995**, *117*, 233−244.

(44) McCullough, R. D.; Tristram-Nagle, S.; Williams, S. P.; Lowe, R. D.; Jayaraman, M. Self-Orienting Head-to-Tail Poly(3-alkylthiopehenes): New Insights on Structure-Property Relationships in Conducting Polymers. *J. Am. Chem. Soc.* **1993**, *115*, 4910−4911.

(45) Burkhart, B.; Khlyabich, P. P.; Thompson, B. C. Influence of the Ethylhexyl Side-Chain Content on the Open-Circuit Voltage in rr-Poly(3-hexylthiophene-co-3-(2-ethylhexyl)thiophene) Copolymers. *Macromolecules* **2012**, *45*, 3740−3748.

(46) Zhang, Y.; Tajima, K.; Hashimoto, K. Nanostructure Formation in Poly(3-hexylthiophene-block-3-(2-ehtylhexyl)thiophene)s. *Macromolecules* **2009**, *42*, 7008−7015.

(47) Ho, V.; Boudouris, B. W.; Segalman, R. A. Tuning Polythiophene Crystallization through Systematic Side Chain Functionalization. *Macromolecules* **2010**, *43*, 7895−7899.

(48) Qi, B.; Wang, J. Fill Factor in Organic Solar Cells. *Phys. Chem. Chem. Phys.* **2013**, *15*, 8972−8982.

(49) Mihailetchi, V. D.; van Duren, J. K. J.; Blom, P. W. M.; Hummelen, J. C.; Janssen, R. A. J.; Kroon, J. M.; Rispens, M. T.; Verhees, W. J. H.; Wienk, M. M. Electron Transport in a Methanofullerene. *Adv. Funct. Mater.* **2003**, *13*, 43−46.

(50) Blom, P. W. M.; deJong, M. J. M.; vanMunster, M. G. Electric-Field and Temperature Dependence of the Hole Mobility in Poly(p-phenylene vinylene). *Phys. Rev. B* **1997**, *55*, 656−659.

(51) Tanase, C.; Blom, P.; de Leeuw, D. Origin of the Enhanced Space-Charge-Limited Current in Poly(p-phenylene vinylene). *Phys. Rev. B* **2004**, *70*, 193202.

(52) Vandewal, K.; Gadisa, A.; Oosterbaan, W. D.; Bertho, S.; Banishoeib, F.; Severen, I. V.; Lutsen, L.; Cleij, T. J.; Vanderzande, D.; Manca, J. V. The Relation Between Open-Circuit Voltage and the Onset of Photocurrent Generation by Charge-Transfer Absorption in Polymer: Fullerene Bulk Heterojunction Solar Cells. *Adv. Funct. Mater.* **2008**, *18*, 2064−2070.

(53) Wang, H.; Shah, M.; Canesan, V.; Chabinyc, M. L.; Loo, Y.-L. Tail State-Assisted Charge Injection and Recombination at the Electron-Collecting Interface of P3HT:PCBM Bulk-Heterojunction Polymer Solar Cells. *Adv. Energy. Mater.* **2012**, *12*, 1447−1455.